

This is the accepted manuscript made available via CHORUS. The article has been published as:

Fulde-Ferrell-Larkin-Ovchinnikov pairing induced by a Weyl nodal line in an Ising superconductor with a high critical field

Xiaoming Zhang and Feng Liu

Phys. Rev. B **105**, 024505 — Published 6 January 2022

DOI: [10.1103/PhysRevB.105.024505](https://doi.org/10.1103/PhysRevB.105.024505)

Fulde-Ferrell-Larkin-Ovchinnikov pairing induced by Weyl nodal lines in Ising superconductors

Xiaoming Zhang^{1,*} and Feng Liu^{2,*}

¹ *College of Physics and Optoelectronic Engineering, Ocean University of China, Qingdao, Shandong 266100, China*

² *Department of Materials Science and Engineering, University of Utah, Salt Lake City, Utah 84112, USA*

*Correspondence to: fliu@eng.utah.edu, zxm@ouc.edu.cn

Superconductivity and electron topology are two quantum phenomena attracting much interest but no causal relationship between them has been reported, since superconductivity is a many-body effect due to electron-electron interaction while the topology is a single-particle manifestation of electron states. Here, we demonstrate electron topology can induce Fulde-Ferrell-Larkin-Ovchinnikov (FFLO) pairing in Ising Bardeen-Cooper-Schrieffer (IBCS) superconductors. Specifically, we predict that the nonmagnetic metals of MA_2Z_4 family, including α_1 -TaSi₂P₄, α_1 -TaSi₂N₄, α_2 -TaGe₂P₄, α_1 -NbSi₂P₄, and α_2 -NbGe₂P₄ monolayers, are all IBCS superconductors with a transition temperature ranging from few to tens Kelvin. The intrinsic IBCS pairing alone will enhance in-plane critical field B_c to ~ 20 -60 times of Pauli limit B_p , and the extrinsic FFLO pairing evoked by topological Weyl nodal lines under magnetic field can further double the B_c/B_p ratio. Our findings not only enrich the fundamental relationship between superconductivity and electron topology, but also affords an effective approach to enhance the robustness of superconductivity.

I. INTRODUCTION

Superconductivity [1] and electron topology [2,3] are two landmark breakthroughs in the fields of condensed matter physics and material science. When they are brought together by proximity effect [4,5], or coexist in one material, e.g., superconductors with topological states [6-8] and *vice versa* [9], a more exotic quantum state of topological superconductivity arises, offering a promising route to fault-tolerant Majorana-based quantum computing [10,11]. However, conventional wisdom tells that there is no causal relationship between superconductivity and electron topology. This is understandable because the former is a many-body effect manifesting an attractive electron-electron interaction of Cooper pairs [12], while the latter is a single-particle effect induced by parity inversion in electron band structure [13]. Surprisingly, here we reveal a novel form of Fulde-Ferrell-Larkin-Ovchinnikov (FFLO) superconducting pairing [14,15], induced by topological Weyl nodal lines in the family of two-dimensional (2D) Ising superconductors of MA_2Z_4 monolayers [16,17]. It not only sheds new light on our fundamental understanding of superconductivity in relation with topology, but also provides a promising approach to enhance the robustness of superconductors.

In addition to critical transition temperature (T_c), another important figure of merit for superconductivity is critical magnetic field (B_c) beyond which the superconductivity vanishes. Generally, magnetic field destroys superconductivity through orbital and/or Pauli paramagnetic mechanisms. Because the orbital effect is weak or absent in those materials with large electron mass [18] or low dimensionality [19], suppressing Pauli effect has been the focus to increase B_c . In particular, the FFLO pairing [14,15,20-25] has been long shown as a feasible mechanism to enhance B_c beyond the Pauli paramagnetic limit (B_p). The formation of FFLO pairs, with non-zero momentum, stems from the spin-non-degenerate Fermi surfaces (FSs) induced by external magnetic field [20,21]. They are favored by low-dimensionality, anisotropic FS and nesting [26], tending to infinity at 1D limit at low temperature. The FFLO pairing has been mainly found in quasi-2D clean-limit superconductors, such as organic [21], Cuprate [22], iron-based [23], heavy-fermion superconductors [20], and van der Waals (vdW) layered NbS_2 [24,25].

On the other hand, recent studies have shown significantly enhanced B_c in 2D Ising Bardeen-Cooper-Schrieffer (IBCS) superconductors [27-37], which suppresses the Pauli pair-breaking effect by an effective out-of-plane Zeeman field (B_{eff}), induced by spin-orbit-coupling (SOC) together with inversion asymmetry (Type-I) [27-30], or with multiple degenerate orbitals (Type-II) [31-33,37]. Such mechanisms have been identified in transition-metal dichalcogenides (TMD) monolayers [27-30,32,34-36], few-layer stanene [33] and Pb films [37], to increase B_c several times over B_p . Here, we demonstrate the coexistence of both IBCS and FFLO pairing in one material, the 2D MA_2Z_4 monolayer. It is made possible by the coexistence of 2D spin-valley-locking bands and 1D Weyl nodal lines in the vicinity of the Fermi level. The 2D FSs around K (K') and Γ support IBCS pairing by the spin-valley locking (Fig. 1a), while the “effective 1D FSs” arising from the Weyl nodal lines along M- Γ -M' enable FFLO

pairing under magnetic field (Fig. 1b). The latter is attributed to the field lifting the degeneracy of Weyl nodal lines to generate spin-polarized electrons (anti-)parallel to the field direction (green colored FS in Fig. 1b), which are no longer favored for IBCS pairing when the field is close to or exceeds B_p . Instead, inhomogeneous FFLO pairing with a finite \mathbf{q} starts to emerge between these spin-polarized electrons on three 1D FSs along the M - Γ - M' paths (Fig. 1b), where the local B_{eff} is weakest. Importantly, the FFLO pairing formed on 1D FS has the maximum stability [20,21].

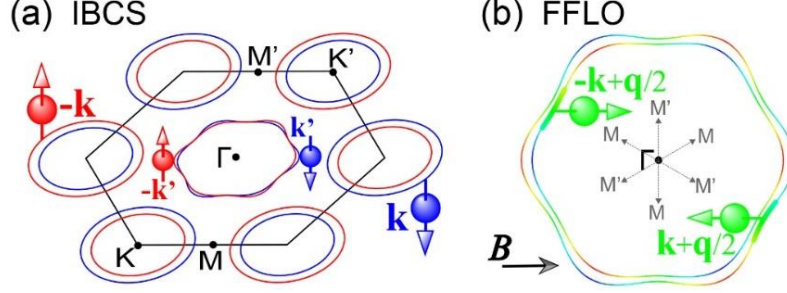


Figure 1. Schematic illustration of superconducting pairing on the FSs of MA_2Z_4 monolayer. (a) IBCS pairing on all FS contours; (b) FFLO pairing on the FS contour around Γ point. Red and blue lines denote respectively the out-of-plane up- and down-spin states, while the green color indicates the states with nearly zero out-of-plane and large in-plane spin-polarization due to the in-plane magnetic field B .

It is worth mentioning that centimeter-scale monolayer films of MoSi_2N_4 and WSi_2N_4 have already been synthesized recently by chemical vapor deposition [16], which opens up a large family of 2D vdW layered materials with the general formula of MA_2Z_4 [16,17] that has no 3D bulk counterparts [38]. Extensive computational research shows that the MA_2Z_4 monolayers generally exhibit outstanding mechanical, thermal, electronic, optical, piezoelectric, thermoelectric, optoelectronics, and photocatalytic properties [16,17,39-44]. Of particular interest to us, certain MA_2Z_4 compounds have been theoretically predicted to be intrinsic superconductors without charge density wave (CDW) instability [17]. Since the MA_2Z_4 monolayers lacking inversion symmetry possess similar Zeeman-type spin-valley locking as the MoS_2 -family monolayers [17,42-44], one might expect that if superconducting, they may have a high B_c . Lo and behold, we found that some superconducting 2D MA_2Z_4 monolayers have the highest B_c/B_p ratio to date, to the best of our knowledge.

Our discovery is partly enabled by our recent development of a first-principles computational approach for superconductivity [45], by self-consistently solving superconducting gap equation constructed from density-functional-theory based Wannier functions (WFs) and electron-phonon coupling (EPC) calculations, especially in the presence of external magnetic field (see details from Note S1 of Supplemental Material (SM) [46]). It allows us to predict not only T_c but also B_c of a superconductor, as well as topological superconductors [45,72,73]. To benchmark this newly developed method, we first solved self-consistently the critical magnetic field of electron-doped

WS₂, whose superconductivity properties are already experimentally available for comparison [36]. Our calculated results reproduce very well the experimental results, especially the measured enhancement of critical field B_c/B_p ratio (see Note S2 of SM [46]). This gives us confidence in making new predictions for MA₂Z₄, since they share same crystal symmetry and similar band structure with WS₂. Also, both systems possess the same spin-valley locking features near the K (K') point giving rise to IBCS pairing. In fact, WS₂ has also Weyl nodal lines along Γ -M paths, but they lie way below the Fermi level (Fig. S1a [46]), so that they do not contribute to superconductivity. This makes WS₂ a Type-I Ising superconductor with solely IBCS pairing. Differently, the Γ -M nodal lines in the considered MA₂Z₄ lie right at the Fermi level, which has led to our discovery of the Weyl-induced FFLO pairing and its effect on enhancing critical magnetic field.

We have systematically investigated the field-dependent superconductivity of α_1 -TaSi₂P₄, α_1 -TaSi₂N₄, α_2 -TaGe₂P₄, α_1 -NbSi₂P₄, and α_2 -NbGe₂P₄ monolayers. We found that without magnetic field, T_c is ~ 22.5 K for α_1 -TaSi₂N₄ and below 10 K for others. The critical field near zero Kelvin (0 K) is estimated to be ~ 70 and ~ 100 times of B_p respectively for α_1 -TaSi₂P₄ and α_2 -TaGe₂P₄, and reach ~ 20 -30 times for others, due to the cooperation of the IBCS and FFLO mechanisms. By fitting the self-consistently calculated B_c/B_p ratios at different temperatures using an extended microscopic model of Ising superconductor, the FFLO pairing on the FS around Γ point was demonstrated to show significant enhancements on the B_c/B_p of α_1 -TaSi₂P₄, α_1 -TaSi₂N₄, α_2 -TaGe₂P₄, and α_2 -NbGe₂P₄ monolayers, while the enhancement is negligible for the α_1 -NbSi₂P₄ monolayers. This is attributed to the fact that the “effective 1D FS” associated with the Weyl nodal lines, which favors the FFLO pairing, is closely related to the strength of Ising SOC, and too weak an SOC, as in α_1 -NbSi₂P₄, is unable to maintain the 1D FS under magnetic field.

II. RESULTS AND DISCUSSION

A. Superconductivity under magnetic field

The atomic structures of MA₂Z₄ monolayer can be viewed as the MoS₂-type MZ₂ monolayer with the surface dangling bonds passivated by InSe-type A₂Z₂, constituting a septuple layer of Z-A-Z-M-Z-A-Z [16,17]. This unique sandwich structure creates a large MA₂Z₄ family with diverse properties arising from varying compositions and relative positions between atomic planes. Here we focus on the nonmagnetic metal compounds which are stable in the α_1 and α_2 phases, including α_1 -TaSi₂P₄, α_1 -TaSi₂N₄, α_2 -TaGe₂P₄, α_1 -NbSi₂P₄, and α_2 -NbGe₂P₄ [17]. From Fig. 2a and 2b, one sees that these non-centrosymmetric phases lack inversion symmetry but contain out-of-plane mirror symmetry m_z . Consequently, SOC induces a B_{eff} to orient electron spins in the out-of-plane direction, manifesting a Zeeman-type spin-valley locking [17,42-44]. This feature can be clearly seen from Fig. 2c-d and Fig. S2, as obtained from the first-principles

calculations (Note S1 of SM [46]). Moreover, the up- and down-spin branches cross with each other along the $M'-\Gamma-M$ \mathbf{k} -point paths, forming three m_z -protected Weyl nodal lines (see theoretical analysis in Note S3 of SM [46]). The generic metallic nature with large Ising spin-splitting at the Fermi level provides the precondition for the intrinsic IBCS pairing, while the 1D Weyl states are shown to initiate and stabilize the extrinsic FFLO pairing under magnetic field by lifting spin degeneracy [20,21,74].

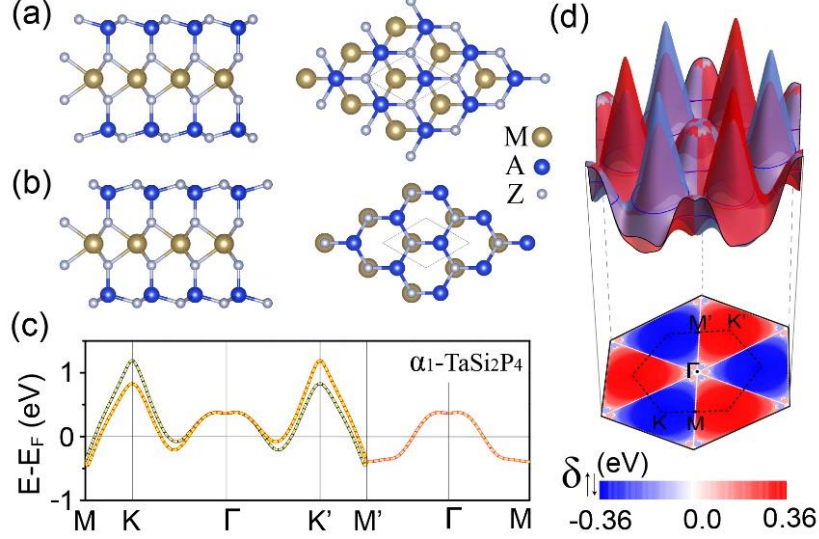


Figure 2. The atomic and electronic structures. Side (left) and top (right) views of (a) α_1 -MA₂Z₄ and (b) α_2 -MA₂Z₄ monolayer. (c) Band structure of α_1 -TaSi₂P₄ monolayer, showing typical features of spin-valley locking and Weyl nodal lines. Red and blue lines denote respectively the split out-of-plane up- and down-spin states, while the pink line indicates the spin-degenerated Weyl nodal line. Yellow dashed lines are the WF fits of band structure. (d) 3D band structure (top panel) plot and 2D distribution of spin-splitting $\delta_{\uparrow\downarrow} = E_{\uparrow} - E_{\downarrow}$ (bottom), i.e. the effective Zeeman field $B_{eff} = \delta_{\uparrow\downarrow}/\mu_B$ for the two metallic bands, which vanishes along the $M'-\Gamma-M$ paths (white lines).

To quantitatively characterize the anticipated superconductivity in MA₂Z₄ monolayers, we first calculated the EPC strength λ and estimated critical temperature T_c^{AD} using the Allen-Dynes (AD) modified McMillan's formula (see Note S1 of SM [46]). Specifically, taking α_1 -TaSi₂P₄ as an example, the calculated phonon spectra (Fig. 3a) indicates that EPC induces a phonon mode softening, but no CDW instability which is known to be detrimental to IBCS [29,30,34,35] and FFLO pairing [74]. The CDW instability is still absent when temperature is increased to 100 K (Note S4 and Fig. S3 in SM [46]). The total EPC λ is calculated to be 0.77 from the cumulative EPC $\lambda(\omega)$ (Fig. 3b), which stems mainly from the couplings between the in-plane phonon vibrations of Ta and the electrons on the d_{xy} , $d_{x^2-y^2}$, and d_{z^2} orbitals of Ta atom (Fig. S4 [46]). With the logarithmically averaged frequency $\langle\omega\rangle_{log}$ being evaluated to be 105.56 K from the Eliashberg spectral function $\alpha^2F(\omega)$ (Fig. 3b), the T_c^{AD} was estimated to be ~ 4.60 K. The key features of α_1 -TaSi₂P₄ are also found in other MA₂Z₄

monolayers (Fig. S5 [46]). We summarize the superconductivity related parameters, e.g. EPC λ , density of states (DOS) at the Fermi level N_F , logarithmically averaged frequency $\langle\omega\rangle_{\log}$, and T_c^{AD} , in Table 1. The convergence of these values was carefully checked (Table S1 and S2 [46]). Qualitatively, the finite T_c^{AD} (Table 1) indicates that all five MA_2Z_4 monolayers are likely to exhibit intrinsic superconductivity without the need of doping.

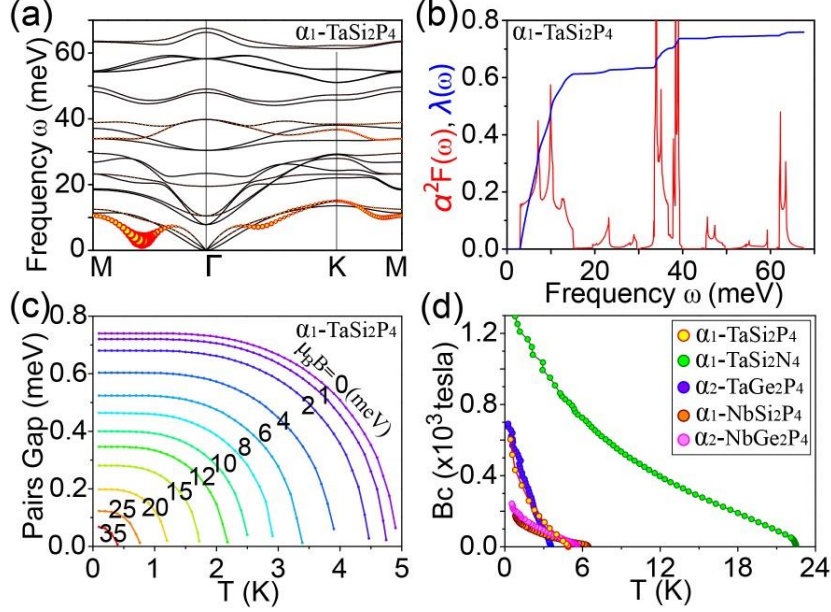


Figure 3. The superconductivity under in-plane magnetic field. (a) Phonon spectra with the magnitude of the EPC strength λ_{qv} being drawn proportional to the size of yellow filled circles. (b) Plots of Eliashberg spectral function $\alpha^2F(\omega)$ and cumulative frequency-dependent EPC strength $\lambda(\omega)$. (c) The temperature-dependent pairing gaps under different in-plane magnetic fields (color bar). (d) The temperature dependent in-plane critical magnetic field for the five MA_2Z_4 monolayers.

Table 1. The parameters related to the superconductivity of MA_2Z_4 monolayers.

	α_1 -TaSi ₂ P ₄	α_1 -TaSi ₂ N ₄	α_2 -TaGe ₂ P ₄	α_1 -NbSi ₂ P ₄	α_2 -NbGe ₂ P ₄
λ	0.77	1.29	0.66	0.79	0.80
N_F (eV ⁻¹)	2.04	1.92	1.96	2.22	2.18
$\langle\omega\rangle_{\log}$ (K)	105.56	231.17	105.48	136.93	115.25
T_c^{AD} (K)	4.60	22.46	3.12	6.31	5.35

Since the above conventional first-principles methods of estimating critical temperature cannot be applied to the systems without time-reversal symmetry, we next further investigate the superconductivity and its dependence on in-plane magnetic field for the five MA_2Z_4 monolayers, by the newly developed method of self-consistently solving the first-principles WF gap equation (see Note S5 of SM [46]). We note that for 2D Ising superconductors under a perfectly aligned in-plane field, orbital de-pairing mechanism can be neglected, then there is only one in-plane critical field B_c above which superconductivity vanishes [27,33,37]. Thus, in the present study, only the suppressing effect of Pauli paramagnetic mechanisms on superconductivity is considered.

Without magnetic field, the self-consistently calculated critical temperature T_c^{SCF} agrees well with T_c^{AD} for those MA_2Z_4 monolayers with intermediate EPC strength $\lambda < 1.0$, which gives a good starting point to perform further calculations with magnetic field by employing the evaluated pairing strength g (Table 2). But for α_1 -TaSi₂N₄ with $\lambda=1.29$, a case of strong EPC, $T_c^{\text{SCF}} \sim 47.00$ K is obtained by using the evaluated $g=0.57$, which overestimates by about two times compared with $T_c^{\text{AD}} \sim 22.46$ K. This indicates that the first-principles WF gap equation can be safely applied only to superconductors with intermediate EPC strength. We thus purposely reduce the g to 0.41 for α_1 -TaSi₂N₄ to reproduce T_c^{AD} for investigating its field dependent superconductivity.

Table 2. The parameters used to calculate and analyze the superconductivity of MA_2Z_4 monolayers with IBCS and FFLO pairing under magnetic field.

	α_1 -TaSi ₂ P ₄	α_1 -TaSi ₂ N ₄	α_2 -TaGe ₂ P ₄	α_1 -NbSi ₂ P ₄	α_2 -NbGe ₂ P ₄
g	0.28	0.41	0.23	0.27	0.27
T_c^{SCF} (K)	4.90	22.50	3.55	6.45	5.60
$\delta_{\text{F}\uparrow\downarrow}^{\text{K}(\text{K}')} \text{ (meV)}$	~ 179.7	~ 197.1	~ 171.5	~ 59.1	~ 59.6
$\delta_{\text{F}\uparrow\downarrow}^{\text{F}}$ (meV)	~ 31.0	~ 46.1	~ 64.8	~ 5.1	~ 15.4
$\tilde{\beta}_{\text{SOC}}^{\text{K}(\text{K}')} \text{ (meV)}$	40	80	40	30	20

Figure 3c shows the calculated pairing gap Δ of α_1 -TaSi₂P₄ as a function of temperature T and in-plane field B . When $B=0$, the pairing gap at 0 K is $\Delta_0 \sim 0.74$ meV, which is fully suppressed at $T_c^{\text{SCF}} \sim 4.90$ K, in good agreement with $T_c^{\text{AD}} \sim 4.60$ K. Due to Pauli paramagnetic pair-breaking effect, T_c^{SCF} decreases with the increasing field. The gap is found to close at 0 K when $\mu_B B$ (μ_B is Bohr magneton) is larger than ~ 35

meV, translating to an in-plane critical magnetic field $B_c \sim 600$ tesla for α_1 -TaSi₂P₄ monolayer. Accordingly, $\Delta(T, B)$ is evaluated for α_1 -TaSi₂N₄, α_2 -TaGe₂P₄, α_1 -NbSi₂P₄, and α_2 -NbGe₂P₄ using the parameters listed in Table 1 and 2 (see Fig. S7 [46]), which enables us to extract their B_c vs T (Fig. 3d). In all five cases, the B_c show an upturn when $T \rightarrow 0$ K, consistent with IBCS and/or FFLO mechanism. The B_c at 0 K for α_1 -TaSi₂N₄, α_2 -TaGe₂P₄, α_1 -NbSi₂P₄ and α_2 -NbGe₂P₄ are ~ 1300 , ~ 700 , ~ 170 and ~ 240 tesla, respectively. In general, a higher T_c^{SCF} together with larger Ising spin-splitting $\delta_{F\uparrow\downarrow}^\Gamma$ and $\delta_{F\uparrow\downarrow}^{K(K')}$ on the FSs around Γ and $K(K')$ (Table 2) tend to induce larger B_c .

To give a semi-quantitative measure on the robustness of superconductivity against the field in the five MA₂Z₄ monolayers, we evaluate the normalized critical field by Pauli limit $B_p = \Delta_0/(\sqrt{2}\mu_B)$, i.e. B_c/B_p , as a function of the normalized temperature, T/T_c^{SCF} , as shown by the filled circles in Fig. 4a-e. At 0 K, the B_c/B_p ratio can reach as high as ~ 100 in α_2 -TaGe₂P₄ monolayer (Fig. 4c), and that of α_2 -TaSi₂P₄ exceeds ~ 70 (Fig. 4a). The α_1 -TaSi₂N₄, α_2 -NbGe₂P₄, and α_1 -NbSi₂P₄ possess the B_c/B_p ratio within the range of 20-30 (Fig. 4b, 4d, and 4e). The predicted B_c/B_p ratio are all higher than most known Ising superconductors.

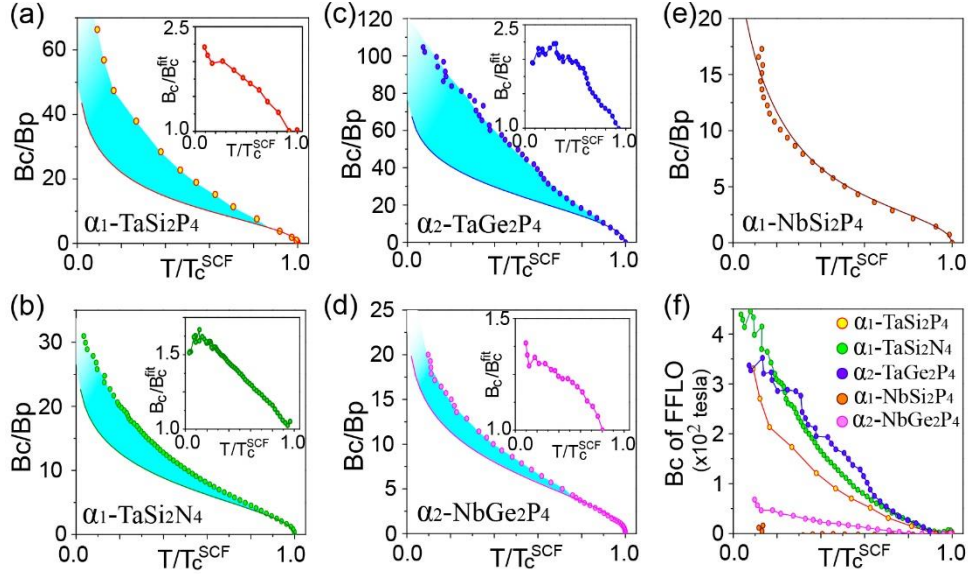


Figure 4. The relative contribution of IBCS and FFLO pairing on field enhancement. (a-e) The dependences of B_c/B_p on normalized temperature T/T_c^{SCF} for (a) α_1 -TaSi₂P₄, (b) α_1 -TaSi₂N₄, (c) α_2 -TaGe₂P₄, (d) α_2 -NbGe₂P₄, and (e) α_1 -NbSi₂P₄ monolayer, which are fitted by the extended microscopic model at low field (solid lines). Light blue shaded regions represent the component of critical field enhanced by additional FFLO pairing. Inset shows the value of the self-consistently calculated total critical fields (B_c) overlaid with model fitted values (B_c^{fit} , i.e. contribution of IBCS pairing) at different temperatures. (f) The normalized temperature dependent field enhancement of FFLO pairing estimated roughly by subtracting the B_c^{fit} from the total enhancement B_c .

B. Analysis of high critical field.

In order to better understand the physical origin of such a high critical field, we extend the conventional microscopic model of Ising superconductor with one effective Ising SOC strength [32,33,37,75] to the case with different SOC strengths (see Note S6 of SM [46]), which resulted in the following equations:

$$F(\mu_B B_c, \tilde{\beta}_{\text{SOC}}^\Gamma) + 2 \times F(\mu_B B_c, \tilde{\beta}_{\text{SOC}}^{K(K')}) = 0 \quad (1)$$

$$F(\mu_B B_c, \tilde{\beta}_{\text{SOC}}) \equiv \ln(T/T_c) + \frac{(\mu_B B_c)^2}{(\tilde{\beta}_{\text{SOC}})^2 + (\mu_B B_c)^2} \text{Re} \left[\psi \left(\frac{1}{2} + \frac{i \sqrt{(\tilde{\beta}_{\text{SOC}})^2 + (\mu_B B_c)^2}}{2\pi k_B T} \right) - \psi \left(\frac{1}{2} \right) \right] \quad (2)$$

Here $\psi(X)$ is the digamma function. It enables us to estimate the in-plane critical field of IBCS pairing for MA_2Z_4 monolayers, which consist of one FS with the effective Ising SOC strength of $\tilde{\beta}_{\text{SOC}}^\Gamma$ and two FSs with $\tilde{\beta}_{\text{SOC}}^{K(K')}$. The $\tilde{\beta}_{\text{SOC}}^\Gamma$ and $\tilde{\beta}_{\text{SOC}}^{K(K')}$ are closely related to the average magnitude of the Ising spin-splitting $\delta_{F\uparrow\downarrow}^\Gamma$ and $\delta_{F\uparrow\downarrow}^{K(K')}$ on the FSs around Γ and $K(K')$, respectively (Table 2). Without losing generality, we set $\tilde{\beta}_{\text{SOC}}^\Gamma = \tilde{\beta}_{\text{SOC}}^{K(K')} \times \delta_{F\uparrow\downarrow}^\Gamma / \delta_{F\uparrow\downarrow}^{K(K')}$ and tune the value of $\tilde{\beta}_{\text{SOC}}^{K(K')}$ to fit the self-consistent solutions at low field, where the IBCS pairing is dominant over the FFLO pairing.

The dependences of B_c/B_p on T/T_c^{SCF} for the five MA_2Z_4 monolayers are fitted using the values of $\tilde{\beta}_{\text{SOC}}^{K(K')}$ summarized in Table 2. Taking $\alpha_1\text{-TaSi}_2\text{P}_4$ as an example (Fig. 4a), one can clearly see the dependence can be well reproduced at low magnetic field. When further enhancing the field, a significant deviation between the extended microscopic model and the self-consistent solution emerges, which increases with the increasing field noticeably. This is because more and more FFLO pairs start to form, as more electron spins in the vicinity of Weyl nodal lines will be re-oriented with those having zero out-of-plane component to satisfy the FS nesting condition (green color in Fig. 1b). It clearly illustrates that the additional FFLO pairing can indeed further enhance the robustness of superconductivity under magnetic field (light blue shaded region in Fig. 4a), by as much as doubling the critical field enhanced by IBCS pairing (inset of Fig. 4a). Similar analysis is applied to $\alpha_1\text{-TaSi}_2\text{N}_4$ (Fig. 4b), $\alpha_2\text{-TaGe}_2\text{P}_4$ (Fig. 4c), and $\alpha_2\text{-NbGe}_2\text{P}_4$ (Fig. 4d) monolayer. However, the enhancement of FFLO pairing is negligible for $\alpha_1\text{-NbSi}_2\text{P}_4$ monolayer, since the self-consistent solution can be well fitted by the extended model of IBCS pairing over the full temperature range (Fig. 4e).

We quantify the critical field enhanced by FFLO pairing in Fig. 4f. One sees that the FFLO pairing alone can increase the critical field by more than ~ 300 , ~ 400 , ~ 300 ,

~ 50 , and ~ 0 tesla for α_1 -TaSi₂P₄, α_1 -TaSi₂N₄, α_2 -TaGe₂P₄, α_2 -NbGe₂P₄, and α_1 -NbSi₂P₄ monolayer at the 0 K limit, respectively. We argue that the FFLO pairing formed on the “effective 1D FS” associated with Weyl nodal line is closely related to the strength of Ising SOC quantified by $\delta_{F\uparrow\downarrow}^\Gamma$ (Table 2). Too weak an SOC is unable to maintain the “1D FS” under magnetic field, such as the case of α_1 -NbSi₂P₄ with negligible FFLO pairing. This demonstrated the critical role that the 1D Weyl nodal lines play in inducing FFLO pairing in a system with strong SOC.

It is worth noting that even without FFLO pairing, the B_c/B_p ratios are still higher than most of the experimentally confirmed Ising superconductors except WS₂ [36]. This is likely because the MA₂Z₄ monolayer neither possesses CDW instability nor needs ionic gating to evoke superconductivity. The novel Weyl-nodal-induced FFLO pairing and the unprecedentedly high critical field in the MA₂Z₄ monolayers may be revealed from field dependence measurements, as previously done for superconductors with either IBCS or FFLO pairing. We emphasize that the MA₂Z₄ monolayers are the first materials in which the field enhancement is enabled by both IBCS and FFLO pairing simultaneously. Also, exploring possible topological superconducting state associated with the Weyl nodal lines, such as the one associated with the Sarma state [76], in these Ising superconductors could be another interesting topic of future study.

III. CONCLUSION

In summary, we have demonstrated the causal relationship between superconductivity and electron topology by revealing a topological Weyl nodal lines induced FFLO pairing in IBCS superconductor MA₂Z₄ monolayer. The superconducting transition temperatures are predicted to ranging from few to tens Kelvin for the considered α_1 -TaSi₂P₄, α_1 -TaSi₂N₄, α_2 -TaGe₂P₄, α_1 -NbSi₂P₄, and α_2 -NbGe₂P₄ monolayers when absenting external magnetic field. At the presence of in-plane field, the cooperation of the IBCS and FFLO mechanisms will enable the B_c/B_p ratio reaching ~ 100 , ~ 70 , ~ 30 , and ~ 20 for α_2 -TaGe₂P₄, α_1 -TaSi₂P₄, α_1 -TaSi₂N₄, and α_2 -NbGe₂P₄ monolayer, respectively. We found the FFLO pairing condensed on the “effective 1D FS” of Weyl nodal line is closely related to the strength of SOC, which is unable to be maintained under magnetic field when the SOC is weak, such as the case of α_1 -NbSi₂P₄ monolayer with negligible FFLO pairing. Our findings not only enrich the fundamental relationship between superconductivity and electron topology, but also affords an effective approach to enhance the robustness of superconductivity against magnetic field.

ACKNOWLEDGMENT

F.L. acknowledges financial support from DOE-BES (No. DE-FG02-04ER46148). X.Z. acknowledges financial support by the National Natural Science Foundation of China (No. 12004357), the Natural Science Foundation of Shandong

Province (No. ZR2020QA053), and the Young Talents Project at Ocean University of China.

References

- [1] D. van Delft and P. Kes, *Phys. Today* **63**, 38 (2010).
- [2] D. J. Thouless, M. Kohmoto, M. P. Nightingale, and M. den Nijs, *Phys. Rev. Lett.* **49**, 405 (1982).
- [3] F. D. M. Haldane, *Phys. Rev. Lett.* **61**, 2015 (1988).
- [4] L. Fu and C. L. Kane, *Phys. Rev. Lett.* **100**, 096407 (2008).
- [5] J.-P. Xu, M.-X. Wang, Z. L. Liu, J.-F. Ge, X. Yang, C. Liu, Z. A. Xu, D. Guan, C. L. Gao, D. Qian, Y. Liu, Q.-H. Wang, F.-C. Zhang, Q.-K. Xue, and J.-F. Jia, *Phys. Rev. Lett.* **114**, 017001 (2015).
- [6] Z. F. Wang, H. Zhang, D. Liu, C. Liu, C. Tang, C. Song, Y. Zhong, J. Peng, F. Li, C. Nie, L. Wang, X. J. Zhou, X. Ma, Q. K. Xue, and F. Liu, *Nat. Mater.* **15**, 968 (2016).
- [7] S. Zhu, L. Kong, L. Cao, H. Chen, M. Papaj, S. Du, Y. Xing, W. Liu, D. Wang, C. Shen, F. Yang, J. Schneeloch, R. Zhong, G. Gu, L. Fu, Y.-Y. Zhang, H. Ding, and H.-J. Gao, *Science* **367**, 189 (2020).
- [8] K.-H. Jin, H. Huang, J.-W. Mei, Z. Liu, L.-K. Lim, and F. Liu, *npj Comput. Mater.* **5**, 57 (2019).
- [9] S. Sasaki and T. Mizushima, *Physica C* **514**, 206 (2015).
- [10] C. Nayak, S. H. Simon, A. Stern, M. Freedman, and S. Das Sarma, *Rev. Mod. Phys.* **80**, 1083 (2008).
- [11] A. Y. Kitaev, *Ann. Phys.* **303**, 2 (2003).
- [12] J. Bardeen, L. N. Cooper, and J. R. Schrieffer, *Phys. Rev.* **108**, 1175 (1957).
- [13] H. Huang and F. Liu, *Research* **2020**, 7832610 (2020).
- [14] P. Fulde and R. A. Ferrell, *Phys. Rev.* **135**, A550 (1964).
- [15] A. Larkin and Y. N. Ovchinnikov, *Sov. Phys. JETP* **20**, 762 (1965).
- [16] Y.-L. Hong, Z. Liu, L. Wang, T. Zhou, W. Ma, C. Xu, S. Feng, L. Chen, M.-L. Chen, D.-M. Sun, X.-Q. Chen, H.-M. Cheng, and W. Ren, *Science* **369**, 670 (2020).
- [17] L. Wang, Y. Shi, M. Liu, A. Zhang, Y.-L. Hong, R. Li, Q. Gao, M. Chen, W. Ren, H.-M. Cheng, Y. Li, and X.-Q. Chen, *Nat. Commun.* **12**, 2361 (2021).
- [18] G. R. Stewart, *Rev. Mod. Phys.* **56**, 755 (1984).
- [19] M. Tinkham, *Introduction to superconductivity* (Courier Corporation, 2004).
- [20] Y. Matsuda and H. Shimahara, *J. Phys. Soc. Jpn* **76**, 051005 (2007).
- [21] J. Wosnitza, *Ann. Phys. Berlin* **530**, 1700282 (2018).
- [22] P. A. Lee, *Phys. Rev. X* **4**, 031017 (2014).
- [23] S. Kasahara, Y. Sato, S. Licciardello, M. Čulo, S. Arsenijević, T. Ottenbros, T. Tominaga, J. Böker, I. Eremin, T. Shibauchi, J. Wosnitza, N. E. Hussey, and Y. Matsuda, *Phys. Rev. Lett.* **124**, 107001 (2020).
- [24] A. Devarakonda, H. Inoue, S. Fang, C. Ozsoy-Keskinbora, T. Suzuki, M. Kriener, L. Fu, E. Kaxiras, D. C. Bell, and J. G. Checkelsky, *Science* **370**, 231 (2020).
- [25] C.-w. Cho, J. Lyu, C. Y. Ng, J. J. He, K. T. Lo, D. Chareev, T. A. Abdel-Baset, M. Abdel-Hafiez, and R. Lortz, *Nat. Commun.* **12**, 3676 (2021).

- [26]J. J. Kinnunen, J. E. Baarsma, J.-P. Martikainen, and P. Törmä, Rep. Prog. Phys. **81**, 046401 (2018).
- [27]J. M. Lu, O. Zheliuk, I. Leermakers, N. F. Q. Yuan, U. Zeitler, K. T. Law, and J. T. Ye, Science **350**, 1353 (2015).
- [28]Y. Saito, Y. Nakamura, M. S. Bahramy, Y. Kohama, J. Ye, Y. Kasahara, Y. Nakagawa, M. Onga, M. Tokunaga, T. Nojima, Y. Yanase, and Y. Iwasa, Nat. Phys. **12**, 144 (2016).
- [29]X. Xi, Z. Wang, W. Zhao, J.-H. Park, K. T. Law, H. Berger, L. Forró, J. Shan, and K. F. Mak, Nat. Phys. **12**, 139 (2016).
- [30]Y. Xing, K. Zhao, P. Shan, F. Zheng, Y. Zhang, H. Fu, Y. Liu, M. Tian, C. Xi, H. Liu, J. Feng, X. Lin, S. Ji, X. Chen, Q.-K. Xue, and J. Wang, Nano Lett. **17**, 6802 (2017).
- [31]C. Wang, B. Lian, X. Guo, J. Mao, Z. Zhang, D. Zhang, B.-L. Gu, Y. Xu, and W. Duan, Phys. Rev. Lett. **123**, 126402 (2019).
- [32]Y. Liu, Y. Xu, J. Sun, C. Liu, Y. Liu, C. Wang, Z. Zhang, K. Gu, Y. Tang, C. Ding, H. Liu, H. Yao, X. Lin, L. Wang, Q.-K. Xue, and J. Wang, Nano Lett. **20**, 5728 (2020).
- [33]J. Falson, Y. Xu, M. Liao, Y. Zang, K. Zhu, C. Wang, Z. Zhang, H. Liu, W. Duan, K. He, H. Liu, J. H. Smet, D. Zhang, and Q.-K. Xue, Science **367**, 1454 (2020).
- [34]S. C. de la Barrera, M. R. Sinko, D. P. Gopalan, N. Sivadas, K. L. Seyler, K. Watanabe, T. Taniguchi, A. W. Tsun, X. Xu, D. Xiao, and B. M. Hunt, Nat. Commun. **9**, 1427 (2018).
- [35]Y. Yang, S. Fang, V. Fatemi, J. Ruhman, E. Navarro-Moratalla, K. Watanabe, T. Taniguchi, E. Kaxiras, and P. Jarillo-Herrero, Phys. Rev. B **98**, 035203 (2018).
- [36]J. Lu, O. Zheliuk, Q. Chen, I. Leermakers, N. E. Hussey, U. Zeitler, and J. Ye, P Natl Acad Sci USA **115**, 3551 (2018).
- [37]Y. Liu, Z. Wang, X. Zhang, C. Liu, Y. Liu, Z. Zhou, J. Wang, Q. Wang, Y. Liu, C. Xi, M. Tian, H. Liu, J. Feng, X. C. Xie, and J. Wang, Phys. Rev. X **8**, 021002 (2018).
- [38]K. S. Novoselov, Natl Sci. Rev. **7**, 1842 (2020).
- [39]B. Mortazavi, B. Javvaji, F. Shojaei, T. Rabczuk, A. V. Shapeev, and X. Zhuang, Nano Energy **82**, 105716 (2021).
- [40]Q. Wang, L. Cao, S.-J. Liang, W. Wu, G. Wang, C. H. Lee, W. L. Ong, H. Y. Yang, L. K. Ang, S. A. Yang, and Y. S. Ang, npj 2D Mater. Appl. **5**, 71 (2021).
- [41]A. Bafekry, M. Faraji, D. M. Hoat, M. Shahrokhi, M. M. Fadlallah, F. Shojaei, S. A. H. Fegghi, M. Ghergherehchi, and D. Gogova, J. Phys. D **54**, 155303 (2021).
- [42]S. Li, W. Wu, X. Feng, S. Guan, W. Feng, Y. Yao, and S. A. Yang, Phys. Rev. B **102**, 235435 (2020).
- [43]H. Ai, D. Liu, J. Geng, S. Wang, K. H. Lo, and H. Pan, Phys. Chem. Chem. Phys. **23**, 3144 (2021).
- [44]C. Yang, Z. Song, X. Sun, and J. Lu, Phys. Rev. B **103**, 035308 (2021).
- [45]X. Zhang, K.-H. Jin, J. Mao, M. Zhao, Z. Liu, and F. Liu, npj Comput. Mater. **7**, 44 (2021).
- [46]See Supplemental Material at <http://> for details of theoretical methods, reproducing the Ising superconductivity of electron-doped WS₂ monolayer, symmetry analyses of the Weyl nodal lines, absence of CDW instability at finite temperature; estimating

critical temperature and magnetic field of MA_2Z_4 monolayers, and extended microscopic model of Ising superconductor with different effective Ising SOC strength, which includes Refs [47-71].

[47]G. Paolo, B. Stefano, B. Nicola, C. Matteo, C. Roberto, C. Carlo, C. Davide, L. C. Guido, C. Matteo, D. Ismaila, C. Andrea Dal, G. Stefano de, F. Stefano, F. Guido, G. Ralph, G. Uwe, G. Christos, K. Anton, L. Michele, M.-S. Layla, M. Nicola, M. Francesco, M. Riccardo, P. Stefano, P. Alfredo, P. Lorenzo, S. Carlo, S. Sandro, S. Gabriele, P. S. Ari, S. Alexander, U. Paolo, and M. W. Renata, *J. Phys.* **21**, 395502 (2009).

[48]S. Baroni, S. de Gironcoli, A. Dal Corso, and P. Giannozzi, *Rev. Mod. Phys.* **73**, 515 (2001).

[49]J. P. Perdew, K. Burke, and M. Ernzerhof, *Phys. Rev. Lett.* **77**, 3865 (1996).

[50]G. Kresse and D. Joubert, *Phys. Rev. B* **59**, 1758 (1999).

[51]W. L. McMillan, *Phys. Rev.* **167**, 331 (1968).

[52]P. B. Allen and R. C. Dynes, *Phys. Rev. B* **12**, 905 (1975).

[53]C. Si, Z. Liu, W. Duan, and F. Liu, *Phys. Rev. Lett.* **111**, 196802 (2013).

[54]A. A. Mostofi, J. R. Yates, G. Pizzi, Y.-S. Lee, I. Souza, D. Vanderbilt, and N. Marzari, *Comput. Phys. Commun.* **185**, 2309 (2014).

[55]B. Peng, H. Zhang, H. Shao, Y. Xu, X. Zhang, and H. Zhu, *RSC Adv.* **6**, 5767 (2016).

[56]Z. Lin, C. Wang, Y. Xu, and W. Duan, *Phys. Rev. B* **102**, 165143 (2020).

[57]Alan J. H. McGaughey and Jason M. Larkin, *Annual Rev. Heat Transfer* **17**, 49-87(2013).

[58]T. Sun, D.-B. Zhang, and R. M. Wentzcovitch, *Phys. Rev. B* **89**, 094109 (2014).

[59]A. Carreras, A. Togo, and I. Tanaka, *Comput. Phys. Commun.* **221**, 221 (2017).

[60]G. Kresse and J. Furthmüller, *Phys. Rev. B* **54**, 11169 (1996).

[61]A. Togo and I. Tanaka, *Scr. Mater.* **108**, 1 (2015).

[62]S. Nosé, *J. Chem. Phys.* **81**, 511 (1984).

[63]W. G. Hoover, *Phys. Rev. A* **31**, 1695 (1985).

[64]S. Kezilebieke, M. N. Huda, V. Vaño, M. Aapro, S. C. Ganguli, O. J. Silveira, S. Głodzik, A. S. Foster, T. Ojanen, and P. Liljeroth, *Nature* **588**, 424 (2020).

[65]G. Sarma, *J. Phys. Chem. Solids* **24**, 1029 (1963).

[66]W. V. Liu and F. Wilczek, *Phys. Rev. Lett.* **90**, 047002 (2003).

[67]E. Gubankova, W. V. Liu, and F. Wilczek, *Phys. Rev. Lett.* **91**, 032001 (2003).

[68]T. Koponen, J. Kinnunen, J. P. Martikainen, L. M. Jensen, and P. Törmä, *New J. Phys.* **8**, 179 (2006).

[69]G. G. Batrouni, M. H. Huntley, V. G. Rousseau, and R. T. Scalettar, *Phys. Rev. Lett.* **100**, 116405 (2008).

[70]H. Suhl, B. T. Matthias, and L. R. Walker, *Phys. Rev. Lett.* **3**, 552 (1959).

[71]A. Gurevich, *Phys. Rev. B* **67**, 184515 (2003).

[72]X. Zhang and F. Liu, *Phys. Rev. B* **103**, 024405 (2021).

[73]X. Zhang, D. Gao, X. Zhu, J. Liu, W. Wang, X. Liu, and M. Zhao, *Phys. Rev. B* **104**, 245409 (2021).

[74]H. Shimahara, *Phys. Rev. B* **50**, 12760 (1994).

- [75] H. Liu, H. Liu, D. Zhang, and X. C. Xie, Phys. Rev. B **102**, 174510 (2020).
- [76] W.-Y. He, B. T. Zhou, J. J. He, N. F. Q. Yuan, T. Zhang, and K. T. Law, Commun. Phys. **1**, 40 (2018).